

# INFLUENCE OF LOADING RATE ON THE FRACTURE BEHAVIOUR OF STEEL FIBER-REINFORCED CONCRETE

X. X. ZHANG\*, A. M. ABD ELAZIM\* G. RUIZ\*, H.M. SALLAM<sup>‡</sup> and Z. CHANG<sup>†</sup>

\* Universidad de Castilla-La Mancha (UCLM)  
ETS de Ingenieros de Caminos, Canales y Puertos  
Avda. Camilo José Cela s/n, 13071 Ciudad Real, Spain  
Email: xiaoxin.zhang@uclm.es - Web page: <http://www.uclm.es>

<sup>‡</sup>Jazan Univsity  
Civil Engineering Department  
Jazan 706, Kingdom of Saudi Arabia  
E-mail: hem\_sallam@yahoo.com

<sup>†</sup> Harbin Engineering University (HEU)  
College of Aerospace and Civil Engineering  
150001 Harbin, China  
Email: changzhongliang@hrbeu.edu.cn - Web page: <http://www.hrbeu.edu.cn>

**Key words:** Steel Fiber-Reinforced Concrete, Loading rates, Drop-weight impact machine, Fracture energy

**Abstract:** Three-point bending tests on notched beams of steel fiber-reinforced concrete (SFRC) have been conducted using both a servo-hydraulic machine and a self-designed drop-weight impact device. The shape and geometry of the specimen followed the RILEM recommendation, i.e., 150 mm × 150 mm in cross section, 700 mm in length, notch-depth ratio was around 1/6 and span was kept constant 500 mm. The peak load and the fracture energy were measured over a wide range of loading rates (loading point displacement rates), spanning six orders of magnitude. Under low loading rates, from  $10^{-3}$  mm/s to  $10^0$  mm/s, the tests were performed with the servo-hydraulic machine; from  $10^2$  mm/s to  $10^3$  mm/s, the drop-weight impact machine was used instead. The results show that the fracture energy and the peak load increase as the loading rate increases. Furthermore, such a trend is relatively mild under low rates. The gain of the fracture energy and peak load is around 10% compared with its quasi-static values. However, under high rates the increases in the fracture energy and the peak load are pronounced due to the inertia effect. The dynamic increase factor of the peak load and the fracture energy is approximately 3.5 and 2.5, respectively.

## 1 INTRODUCTION

Steel fiber-reinforced concrete (SFRC) is concrete made of hydraulic cements containing fine or fine and coarse aggregate and discontinuous discrete steel fibers [1]. Addition of randomly distributed steel fibers improves concrete properties, such as static

flexural strength, ductility and flexural toughness. Some examples of structural and nonstructural uses of SFRC are hydraulic structures, airport and highway paving and overlays, industrial floors, refractory concrete, bridge decks, shotcrete linings and coverings, and thin-shell structures [2].

Besides bearing quasi-static loads, many concrete structures are subjected to short duration loads. Such as the impacts from missiles and projectiles, wind gusts, earthquakes, and machine dynamics. Several techniques have been developed to study the dynamic fracture behaviour of concrete and concrete structures, like modified Charpy impact test, Split Hopkinson pressure bar test, drop-weight impact test and explosive test [3, 4].

Many researchers have shown that the impact resistance can be increased substantially with the addition of randomly distributed steel fibers to concretes. For instance, Namman and Gopalaratnam [5] have used a drop-weight impact machine and an Instron universal machine to study the bending properties of steel fiber-reinforced mortar beams at four different loading rates,  $4.23 \times 10^{-4}$  mm/s, 8.46 mm/s,  $7.0 \times 10^2$  mm/s and  $1.0 \times 10^3$  mm/s, respectively. The dimension of the beam was 12.5 mm  $\times$  75 mm  $\times$  300 mm (width  $\times$  depth  $\times$  length) and the span was 254 mm during the tests. Three volume fractions of fibers (1%, 2% and 3%), three fiber aspect ratios (47, 62 and 100) were adopted. The results showed that depending on the fiber reinforcing parameters the energy absorbed by the composite at static loading rates can be one to two orders of magnitude higher than that of the unreinforced matrix. Moreover, up to a three times increase was observed in the modulus of rupture and the energy absorbed by the composite when the loading rate increases from  $4.23 \times 10^{-4}$  mm/s to  $1.0 \times 10^3$  mm/s. The similar tendency was also obtained by Gopalaratnam and Shah [6].

Banthia [7] has adopted a drop-weight impact machine to conduct dynamic tests on steel fiber-reinforced high-strength concrete beams at loading rate around 4 m/s, the specimen was 100 mm in width, 125 mm in depth and 1200 mm in length over a span 960 mm. The peak bending load and fracture energy got 498% and 640% increases, respectively, compared with their quasi-static values. Later, a modified Charpy impact machine was designed to test concrete and

SFRC in uniaxial tension [8]. The results showed that under impact, the higher strength of the matrix, the less effective the fibers in improving fracture energy absorption.

ACI Committee 544 [3], has proposed another type of drop-weight impact test for evaluating the impact resistance of fiber-reinforced concrete (FRC), i.e., a hammer is dropped repeatedly to impact a disc specimen, and the number of blows required to cause the first visible crack on the top and to cause ultimate failure are both recorded. This method is designed to obtain relative performance of plain concrete and FRC. Natraja et al. [9] analyzed the statistical variation of impact resistance of SFRC under this type of repeated drop impact condition. The disc samples were 150 mm in diameter and 64 mm in thickness and containing 0.5% volume fraction of round crimped steel fibers with 0.5 mm in diameter and 55 in aspect ratio. The observed coefficients of variation were 57% and 46% for the first crack resistance and ultimate resistance, respectively.

Most studies as cited above were concentrated on the unnotched specimens, unlike notched samples, for them, the crack is located close to the notch plane and the nonlinear deformation is negligible in the rest of the specimen. Thus, in 2002, the final recommendation for the bending test for SFRC was presented by the RILEM TC 162-TDF Committee, which improves several aspects of other standards [10]. The test is conducted on notched beams (150 mm  $\times$  150 mm in cross section) with central point loading. One of the greater advantages of such configuration is that it guarantees the stability during the test even for FRC with low fiber contents. In 2005, a similar method was also proposed by EN 14651 standard, two years later, an updated version was available [11].

In order to get additional insights into the loading rate effect on the fracture properties of SFRC, in this paper we present three-point bending tests of notched specimen conducted at a wide range of loading point displacement rates (for simplicity, it is substituted by loading rates), from  $10^{-3}$  mm/s to  $10^3$  mm/s,

using both a servo-hydraulic testing machine and a drop-weight impact instrument. The shape and geometry of the specimen follow RILEM recommendations [10].

The results show that the fracture energy and the peak load increase as the loading rate increases. Moreover, such a trend is relatively mild under low rates. While it is pronounced under high loading rates due to the inertia effect.

The rest of this paper is structured as follows: the experimental procedure is given in Section 2, in Section 3 the results are presented and discussed. Finally, relevant conclusions are drawn in Section 4.

## 2 EXPERIMENTAL PROCEDURE

### 2.1 Material characterization

A single type of SFRC was used throughout the experiments, made with a siliceous aggregate of 12 mm in maximum size and ASTM type II cement, 42.5R. Two types of super plasticizer (Glenium ACE-325, Glenium B-255) were used in the concrete composition. The mixing proportions by weight were shown in 1: 0.29: 0.1: 0.048: 1.6: 1.2: 0.0066: 0.021 (cement: water: limestone filler: silica fume: sand: coarse aggregate: nanosilica: superplasticizer).  $64.5 \text{ kg/m}^3$  of steel fiber were added as the reinforcement. The steel fiber used was hooked-end with 50 mm in length, 0.75 mm in diameter and 67 in aspect ratio, it has a tensile strength 1900 MPa.

Compressive tests were carried out at an age of 65 days, following ASTM C39 (which is analogous to EN 12390-3), cylinders of  $150 \times 300$  mm (diameter  $\times$  height) were used. To perform the compressive tests, a Servo-hydraulic testing machine was adopted. Values of characteristic parameters: the compressive strength ( $f_c$ ), the elastic modulus ( $E$ ) and the Poisson's ratio ( $\nu$ ) are listed in Table 1.

**Table 1:** Properties of the SFRC at an age of 65 days

	$f_c$ (MPa)	$E$ (GPa)	$\nu$	$\rho$ ( $\text{kg/m}^3$ )
Mean	92.1	35.1	0.18	2438
Standard deviation	5	1	0.01	17

### 2.2 Three-point bending tests

To study the mechanical properties of the SFRC prisms, three-point bending tests were conducted on notched beams over a wide loading rate range from  $10^{-3}$  to  $10^3$  mm/s. Two testing machines were adopted to carry out the tests, one was a servo-hydraulic testing machine, and the other was a self-designed drop-weight impact instrument.

The dimensions of the test beams were  $150 \times 150$  ( $B \times D$ ) mm in cross-section, and 700 mm in total length ( $L$ ). The initial notch-depth ratio ( $a/D$ ) was approximately 1/6, and the span ( $S$ ) was fixed at 500 mm during the tests, see Figure 1.

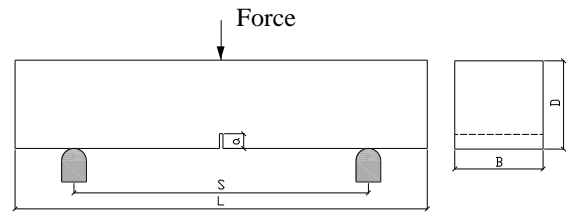


**Figure 1:** Schematic diagram of the specimen.

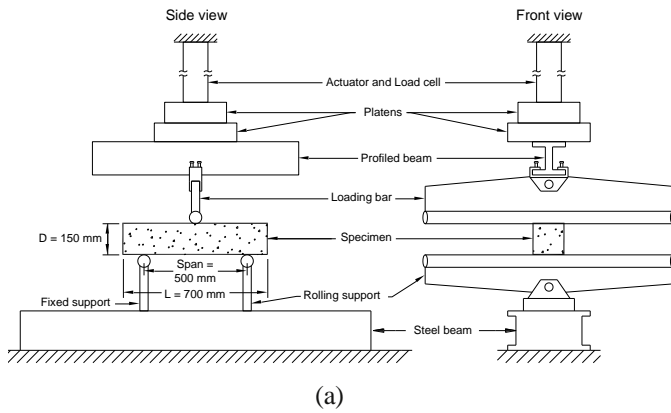
#### 2.2.1 Tests under low loading rates $10^{-3}$ to $10^0 \text{ mm s}^{-1}$

Within this low loading rate range, the tests were performed using the servo-hydraulic testing machine under position control coupled to a robust frame in the Laboratory of Materials and Structures of the Civil Engineering School of the University of Castilla-La Mancha in Ciudad Real as shown in Figure 2. The alignment of the supports and the loading line was checked when installing each specimen. One of the supports was fixed, whereas the other was free to rotate around the axis of the frame.

Three loading rates, from quasi-static level ( $3.33 \times 10^{-3} \text{ mm s}^{-1}$ ) to rate dependent levels (0.1 mm/s and 3.33 mm/s), were applied. Six specimens were tested at each loading rate.

were  $8.81 \times 10^2 \text{ mm/s}$ ,  $1.77 \times 10^3 \text{ mm/s}$  and  $2.66 \times 10^3 \text{ mm/s}$ , respectively. Six specimens were tested at each impact speed. A detailed description of the instrument is given in references [4, 12].

The impact force between the hammer tup and the specimen is measured by a piezoelectric force sensor. Moreover, the reaction force is determined by two force sensors located between the supports and the specimen. An accelerometer bonded to the impact hammer was used to measure acceleration and displacement during the impact process.

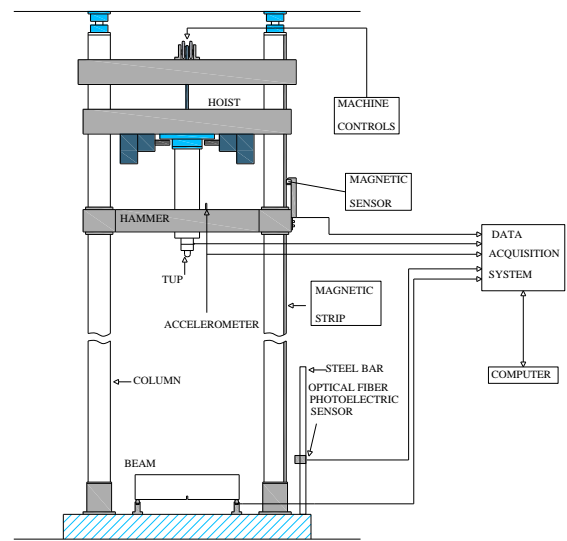


(b)

**Figure 2:** (a) Schematic diagram and (b) photo of the experimental set-up of the servo-hydraulic testing machine.

### 2.2.2 Tests under loading rates from $10^2$ to $10^3 \text{ mm/s}$

In this high loading-rate range, all tests were conducted using the instrumented, drop-weight impact apparatus as shown in Figure 3. It has the capacity to drop a 316 kg mass from heights of up to 2.6 m, and can accommodate flexural specimens with spans of up to approximately 1.6 m. In this study, an impact hammer weighing 120.6 kg was employed and three-drop heights adopted were 40, 160 and 360 mm. The corresponding impact velocities



(a)



(b)

**Figure 3:** (a) Schematic diagram and (b) photo of the drop-weight impact machine.

Due to the fact that the specimen was not broken completely during the test, the area under the load versus displacement at mid-span curve up to a specified deflection was used in the evaluation of fracture energy ( $G_F$ ), similar method was also adopted in some other references [8, 14, 16]. Here, a cut-off point was chosen at the displacement of 2 mm for all the tests under low and high loading rates.  $G_F$  was determined by Eq. (1).

$$G_F = \frac{W_o + mg \frac{S}{L} \delta_s}{B(D-a)} \quad (1)$$

where  $W_o, B, D, a, S, L, m, \delta_s$ , and  $g$  are the area under the experimental load-displacement curve, width, depth, notch, span, length, mass, specified deflection of the beam  $\delta_s$  (2 mm) and gravitational acceleration, respectively. Under dynamic loading conditions,  $W_o$  was obtained by the area under the reaction force – displacement (load – displacement) curves, where the reaction force is evaluated by adding the values from both support data points as proposed in reference [12, 13].

### 3 RESULTS AND DISCUSSION

#### 3.1 Fracture behaviour at a wide range of loading rates

Typical impact and reaction forces versus time curves are shown in Figure 4 (left column). It is worth noting that the time intervals between the start points of the impact force and the reaction force are 344, 250, and 248  $\mu$ s, corresponding to loading rates  $8.85 \times 10^2$ ,  $1.77 \times 10^3$ , and  $2.66 \times 10^3$  mm/s respectively, as they are indicated in the figure. However, it only takes approximately 118  $\mu$ s for the shear stress wave to travel from the impact point to the support point. Thus, there is an apparent time delay. The reason could be the small gap between the support tup and the specimen though the contact between them is “good” by eyesight. It is obvious that the time delay decreases with increase in loading rate, on the contrary, the peak loads of the impact and the reaction forces increase.

Fig. 4 (right column) shows the comparison between the impact and the reaction forces versus displacement curves. The initial time of

the reaction force has been shifted, thus, the impact and the reaction forces have the same starting points. For the tests under drop height 40 mm (loading rate:  $8.85 \times 10^2$  mm/s), the impact energy was too small to deform and fracture the beam apparently as shown in Figure 5 (d), hence, the beam is almost like a fixed end to the impact hammer. According to the stress wave theory, the peak of the reaction force (95.2 kN) is greater than that of the impact force (70.4 kN). Furthermore, for the tests under drop heights 160 mm (loading rate:  $1.77 \times 10^3$  mm/s), the beam was deformed and fractured clearly but not broken completely as shown in Figure 5 (e). The beam undergoes first an acceleration, and then a deceleration before it finally comes to rest. During the deceleration, the peak load of the reaction force will be greater than that of the impact force during this period due to the inertia effect. When the drop height of the hammer was increased to 360 mm (loading rate:  $2.66 \times 10^3$  mm/s), the beam was almost broken entirely as shown in Figure 5 (d), consequently the peak of the reaction force (164.8 kN) is less than that of the impact force (190.1 kN). The former is around 87% of the latter, i.e., majority of the impact force is used to fracture the specimen, only a small portion is keeping balance with the inertia force.

Failure modes of beams under low loading rates are shown in Figure 5 (a, b, c), it can be observed that there are more branch cracks around the main crack compared with the crack pattern of beams in Figure 5 (d, e, f) under high loading rates. Moreover, all beams were not broken completely; the post-peak fracture behaviour of the beam was greatly improved by the addition of steel fibers. Furthermore, all the fibers in the crack surface are pulled out, no single broken fiber is found.

Figure 6 shows the comparison of the typical load–displacement curves at different loading rates. It is obvious that the peak load increases with increase in loading rates. However, the stiffness of the beam does not show a similar tendency, which is due to the sensitivity of the elastic flexibility of the beam to the boundary conditions during the

application of the concentrated load as proposed in reference [14]. Nevertheless, the stiffness still gains a sound increase when the loading rates have a big jump, i.e., from low to high loading rates.

Table 2 provides detailed information about the experimental results. The dynamic increase factor (*DIF*) is defined by the ratios of the peak load ( $P_{max}$ ) and fracture energy to their corresponding quasi-static values. Here, the lowest loading rate ( $\dot{\delta} = 3.33 \times 10^{-3}$  mm/s) is taken as the quasi-static loading condition.  $H$  stands for the drop height of the hammer under impact loading conditions. It is worth noting that the fracture energy under drop height 40 mm was not calculated due to the fact that the maximum displacement was only around 0.5 mm, it did not reach the specified deflection 2 mm as mentioned before.

Figure 7 (a) shows the loading rate effect on the peak load. It is evident that the peak load increases with increase in loading rates. It should be also noted that the tendency is minor under low loading rates, while it is pronounced instead under high loading rates. A prediction equation for this rate effect is derived from the experimental results as shown in Eq. (2).

$$\begin{aligned} P_{max} &= P_{max}^s (1 + k\dot{\delta}^n) \\ &= 53.3 [1 + (7.5 \times 10^{-4})\dot{\delta}^{1.01}] \end{aligned} \quad (2)$$

where  $P_{max}^s$  is the static peak load in kN, coefficients  $k$  and  $n$  are adjusting parameter,  $\dot{\delta}$  is the loading rate in mm/s. The equation can be used to efficiently predict the rate effect on the peak load and could also be helpful in performing numerical simulations. Moreover, the fitting curve gives the static value of the peak load (53.3 kN) as well, and that this could only be obtained by a exactly static test.

The loading rate effect on the fracture energy is shown in Figure 7 (b). The trend is similar to that of the peak load, i.e., the tendency is moderate under low loading rates, while under high loading rates it is dramatic. A similar equation is also proposed to represent this behaviour as shown in Eq. (3).

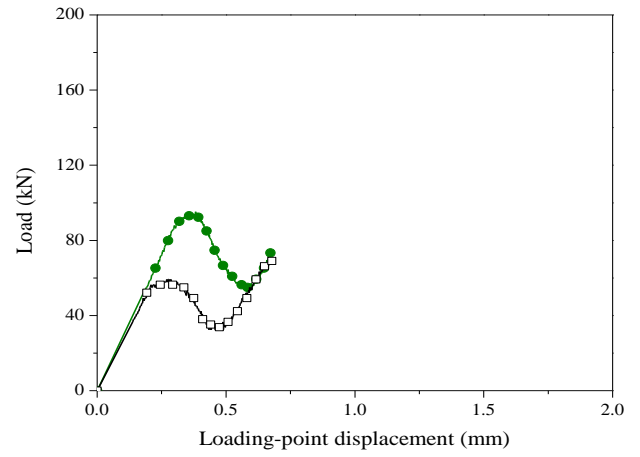
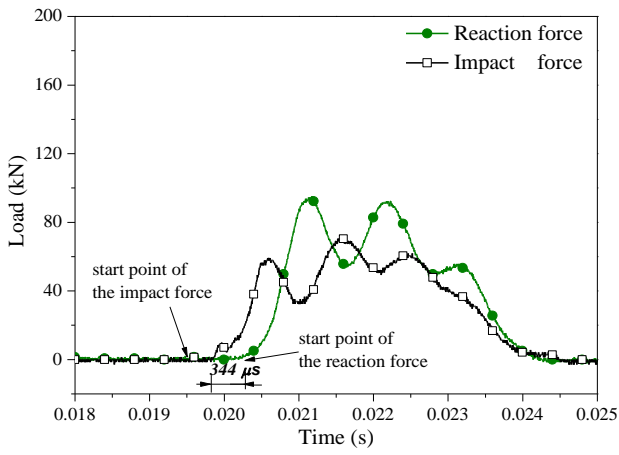
$$\begin{aligned} G_F &= G_F^s (1 + m\dot{\delta}^r) \\ &= 4565.9 [1 + (7.6 \times 10^{-6})\dot{\delta}^{1.54}] \end{aligned} \quad (3)$$

where  $G_F^s$  is the static fracture energy in N/m, coefficients  $m$  and  $r$  are adjusting parameter,  $\dot{\delta}$  is the loading rate in mm/s.

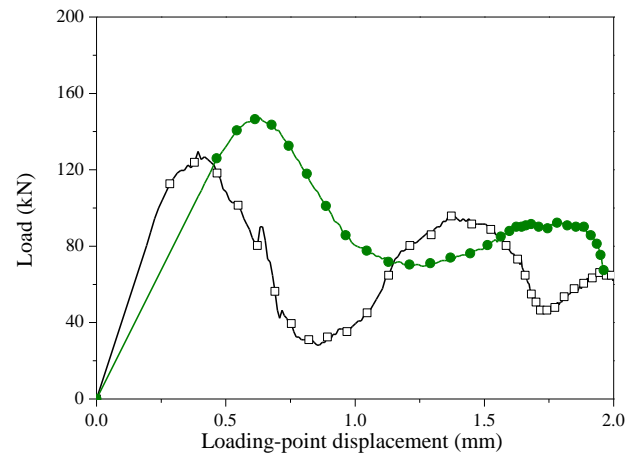
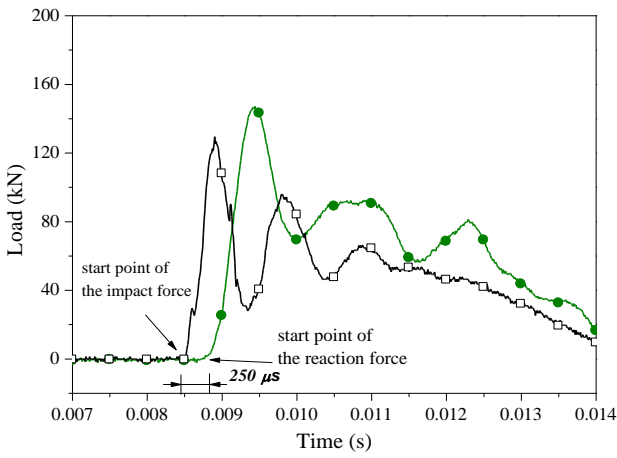
### 3.2 Comparison with data already published

Table 3 provides a comparison of some experimental results from other researches and the results presented in this paper. From this table, it can be observed that the loading rate effect on the mechanical properties of different steel fiber-reinforced concretes is similar.

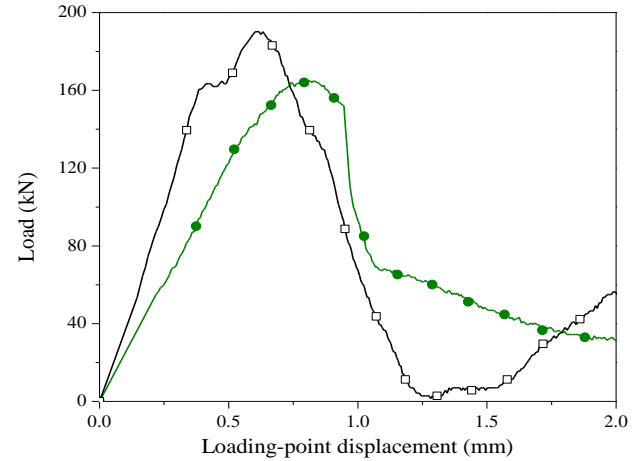
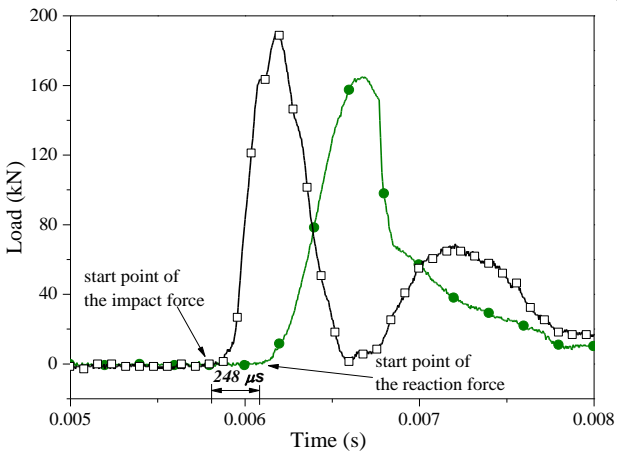
The values of DIF for the peak load and the fracture energy are in the same order of magnitude, though there is some difference among them. Such difference is likely attribute to type, shape and geometry of the steel fiber, fiber volume ratio, bond behaviour between fibers and matrix, size of the specimen and the testing conditions. Furthermore, it should be taken into account as well that the notched specimen absorbs less dissipated energy than that of the unnotched one due to the fact that the crack locates close to the notch plane. Thus, it is better to use notched specimen to study the fracture behaviour of SFRC for reducing the influence of dissipated energy. Recently, Caverzan and Cadoni et al. [17] have investigated the dynamic fracture behaviour of a high performance fiber-reinforced cementitious composite by using a modified Hopkinson bar, the notched cylinder specimens were used in the test. The results showed that the DIF value for the fracture energy was approximately 1.5. It is worth noting that the rate effect on the fracture energy illustrates similar tendency with different loading methods, such as modified Charpy impact testing machine, drop-weight impact instrument and modified Hopkinson bar system.



(a) Loading rate  $8.85 \times 10^2$  mm/s



(b) Loading rate  $1.77 \times 10^3$  mm/s



(c) Loading rate  $2.66 \times 10^3$  mm/s

**Figure 4:** Typical impact and reaction forces versus time (left), and comparison of load versus displacement (right), at loading rates (a)  $8.85 \times 10^2$  mm/s (b)  $1.77 \times 10^3$  mm/s and (c)  $2.66 \times 10^3$  mm/s.

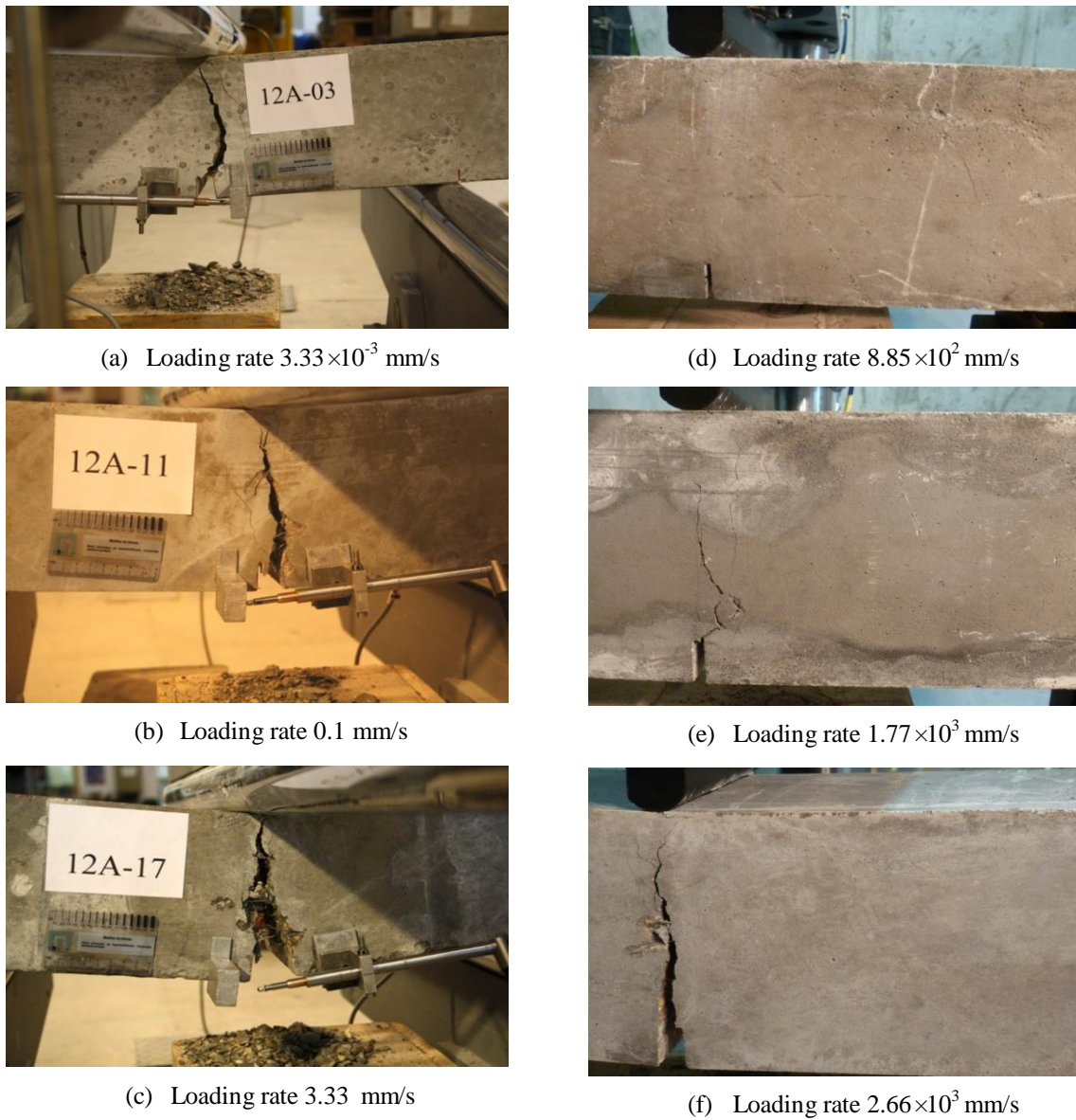


**Figure 5:** Failure modes of SFRC beams under different loading rates.

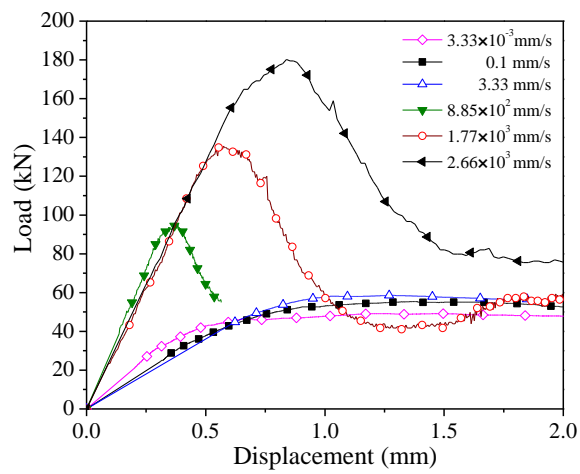
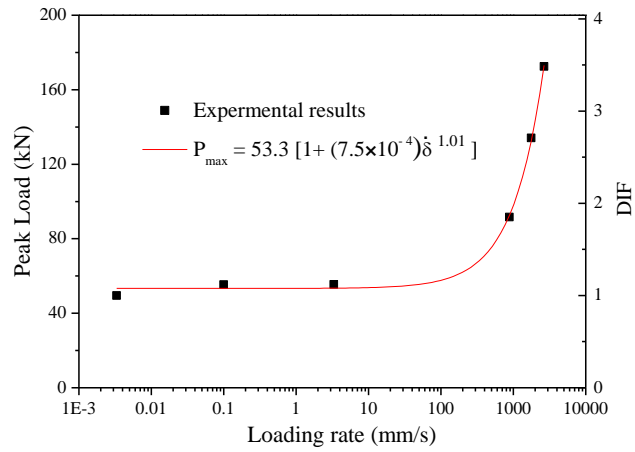


**Figure 6:** Load-displacement curves at different loading rates.

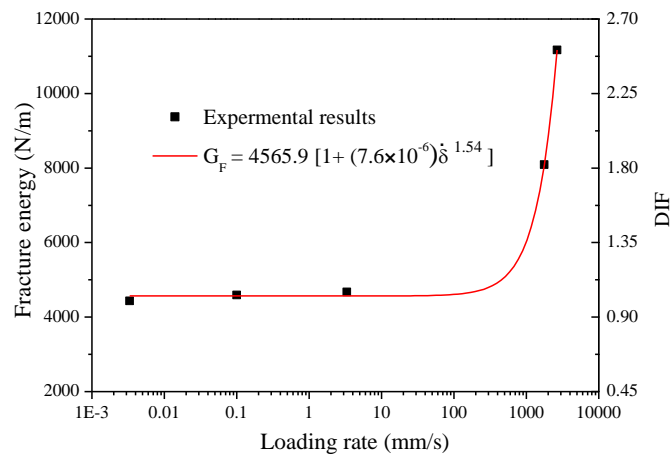
**Table 2:** Experimental results at different loading rates

Testing machine	$H$ (mm)	$\dot{\delta}$ (mm/s)	$P_{max}$ (kN)	$DIF$ for $P_{max}$	$G_F$ (N/m)	$DIF$ for $G_F$	Number of fibers
Servo-Hydraulic testing machine	-	$3.33 \times 10^{-3}$	49.5 (11)	1	4432 (1022)	1	267(59)
	-	0.1	55.4 (4)	1.119	4590 (566)	1.04	283(56)
	-	3.33	55.5 (6)	1.121	4676 (455)	1.06	253(46)
Drop-weight impact machine	40	$8.85 \times 10^2$	91.6 (6)	1.85	-	-	266(31)
	160	$1.77 \times 10^3$	134.1 (6)	2.71	8089 (782)	1.83	264(14)
	360	$2.66 \times 10^3$	172.5 (11)	3.48	11167(1391)	2.52	248(32)

Note: values in parentheses are standard deviations.



(a)



(b)

**Figure 7:** (a) Loading rate dependence of the peak load (b) Loading rate dependence of the fracture energy.

**Table 3:** Comparison of experimental results

	Specimen size (mm) $B \times D \times S$	Notch $a$ (mm)	Fiber content (volume ratio)	Mix proportions $C:S:A:W$	$l/d$ (Aspect ratio)	Steel fiber shape	Dynamic experimental set-up	Hammer weight (kg)	Max velocity (m/s)	$f_c$ (MPa)	$E$ (GPa)	$P_{max}$ (kN)	$G_F$ (N/m)	$DIF$ $P_{max}$	$DIF$ $G_f$
Suaris and Shah, 1983, [15]	38.1×76.2×381	0	1%	1:2:0:0.5	25.4/0.254 (100)	Hooked- end	Drop weight impact	108.9	1.0	57.5	34.5	7.1, (Quasi-static value 3.7)	at a central deflection 12.5 mm 16471, (Quasi- static value 8277)	1.92	1.99
Naaman and Gopalaratnam, 1983, [5]	12.5×75×254	0	1%	1:2:0:0.4	25/0.25 (100)	Smooth brass- coated	Drop weight impact	-	1.0	64.7	-	3.9, (Quasi- static value 1.4)	at a central deflection 12.5 mm 5082, (Quasi- static value 2229)	2.79	2.28
Gopalaratnam and Shah, 1986, [6]	25×64×203	12.5	1%	1:2:0:0.5	25.8/0.41 (63)	Smooth brass- coated	Modified Charpy	-	2.45	30.4	29.2	3.9, (Quasi-static value 2.0)	at a central deflection 2.54 mm, 3010, (Quasi-static value 1710)	1.95	1.76
Banthia, 1987, [7]	150×150×960	0	1.5%	1:2:3.5:0.5	60/0.6 (100)	Hooked- end	Drop weight impact	42.5	3.79	50	-	57.3, (Quasi-static value 11.5)	12724, (Quasi- static value 1991)	4.98	6.40
Current work	150×150×500	25	0.8%	1:2.25:1.5:0.37	50/0.75 (67)	Hooked- end	Drop weight impact	120.6	2.66	79.3	31.0	172.5, (Quasi-static value 48.7)	at a central deflection 2.0 mm, 7963, (Quasi-static value 4276)	3.48	2.52

$C: S: A: W$ ; Cement: Sand: Aggregate: Water, mix proportions by weight.

$B \times D \times S$ ; Width × Depth × Span.

$l/d$ ; Length/diameter of the steel fiber.

## 4 CONCLUSIONS

The fracture behaviour of a steel fiber reinforced concrete under dynamic loading conditions was investigated in this study. The loading rates varied considerably from a quasi-static level to a dynamic level, the order of magnitude changed from  $10^{-3}$  to  $10^3$  mm/s. As a result of the study, the following conclusions can be drawn:

For studying dynamic fracture behaviour of steel fiber-reinforced concrete, it is better to use notched specimen instead of unnotched one, thus, less dissipated energy is found in the specimen.

The peak load and the fracture energy are sensitive to the loading rate. Under low loading rates, the rate effect is minor, while it is pronounced under high loading rates. The dynamic increase factor of the peak load and the fracture energy is approximately 3.5 and 2.5, respectively. This attributes primarily to the strain rate sensitivity of the matrix and the pullout resistance of the fibers.

Two prediction-equations for the rate sensitivity of the fracture energy and the peak load are provided. They are helpful in numerical simulations that evaluate the rate dependence of the fracture behaviour.

## Acknowledgements

The authors thank the INCRECYT and the fellowship under grant No BES-2008-008216.

## REFERENCES

[1] ACI Committee 544, 1996. State-of-art report on fiber reinforced concrete. *ACI Committee 544 report 544.1R-96*. American Concrete Institute. Detroit.

[2] ACI Committee 544, 2008. Guide for Specifying, Proportioning, and Production of Fiber Reinforcing Concrete. *ACI Committee*

*544 report 544.3R-08*. American Concrete Institute. Detroit.

[3] ACI Committee 544, 1989. Measurement of properties of fiber reinforced concrete (*Reapproved 2009*). *ACI Committee 544 report 544.2R-89*. American Concrete Institute. Detroit.

[4] Zhang, X. X., Ruiz, G., and Yu, R. C., 2010. A new drop-weight impact machine for studying fracture processes in structural concrete. *Strain*. **46**: 252-57.

[5] Naaman, A. E., and Gopalaratnam, V. S., 1983. Impact properties of steel fiber reinforced concrete in bending. *International journal of cement composites and lightweight concrete*. **5**: 225-33.

[6] Gopalaratnam, V. S., and Shah, S. P., 1986. Properties of steel fiber reinforced concrete subjected to impact loading. *Journal of the American Concrete Institute*. **83**: 117-26.

[7] Banthia, N., 1987. Impact resistance of concrete. *PhD thesis: Department of Civil Engineering, the University of British Columbia*, Vancouver, Canada.

[8] Banthia, N., Mindess, S., and Trottier, J. F., 1996. Impact resistance of steel fiber reinforced concrete. *ACI Materials Journal*. **93**: 472-79.

[9] Nataraja, M. C., Dhang, N., and Gupta, A. P., 1999. Statistical variations in impact resistance of steel fiber-reinforced concrete subjected to drop weight test. *Cement and Concrete Research*. **29**: 989-95.

[10] RILEM TC 162-TDF, 2002. Test and design methods for steel fiber reinforced concrete - bending test. *Materials and Structures/Materiaux et Constructions*. **35**: 579-82.

[11] UNE-EN 14651-2007, Método de ensayo para hormigón con fibras metálicas – determinación de la Resistencia a la tracción por flexión (límite de proporcionalidad (LOP), Resistencia residual).

[12] Zhang, X.X., Ruiz, G., and Yu, R.C. and Tarifa M., 2009. Fracture behaviour of high-strength concrete at a wide range of loading rates. *International Journal of Impact Engineering*. **36**: 1204-09.

[13] Banthia, N., Mindess, S., Bentur, A., and Pigeon, M., 1989. Impact testing of concrete using a drop-weight impact machine. *Experimental Mechanics*. **29**: 63-9.

[14] Planas, J., Guinea G.V., and Elices M., 1994. Stiffness associated with quasi-concentrated loads. *Materiaux et constructions*. **27**: 311-8.

[15] Suaris, W., and Shah, S., 1983. Properties of concrete subjected to impact. *Structural engineering*. **10**: 1727-41.

[16] Akcay, B., and Tasdemir, M. A., 2012. Mechanical behaviour and fibre dispersion of hybrid steel fibre reinforced self-compacting concrete. *Construction and Building Materials*. **28**: 287-93.

[17] Caverzan, A., Cadoni, E. and Prisco, M., 2012. Tensile behaviour of high performance fibre-reinforced cementitious composites at high strain rates. *International Journal of Impact Engineering*. **45**: 28-38.